Shape Distortion by Irreversible Flux-Pinning-Induced Magnetostriction

T. H. Johansen, J. Lothe, and H. Bratsberg

Department of Physics, University of Oslo, P.O. Box 1048, Blindern, 0316 Oslo 3, Norway
(Received 23 December 1997)

Exact analytical results are obtained for the flux-pinning-induced magnetostriction in cylindrical type-II superconductors placed in parallel magnetic fields. New modes of irreversible deformation are found: In contrast to the circular cylinder where shape is conserved, it is shown that a square cross section deforms with considerable distortion. During a field cycle, concave, convex, and even more complicated distortions are predicted. Strong implications for dilatometric measurements on crystals are emphasized. The main results are valid for any critical-state model, $j_c = j_c(B)$.   [S0031-9007(98)06117-1]

It was discovered by Ikuta and co-workers [1] that high temperature superconductors (HTSCs), when placed in a magnetic field, can respond by a giant magnetostriction. Relative changes in sample size as large as 10^{-4} were observed in single crystals of $Bi_2Sr_2CaCu_2O_8$. To explain this deformation, which is about 2 orders of magnitude larger than values reported for conventional superconductors [2], they considered the stress exerted on the crystal by pinned vortices. Treating the crystal as an infinite slab of half-width w placed in a parallel applied field B_a/μ_0, the pinning-induced magnetostriction in the transverse direction was derived from the critical state model to be

$$\Delta w/w = (2c\mu_0 w)^{-1} \int_0^w [B^2(x) - B_a^2] dx, \quad (1)$$

where c is the elastic constant and $B(x)$ is the local induction. As is evident from Eq. (1), and also pointed out immediately by Ikuta *et al.,* the pinning-induced magnetostriction is intimately related to the magnetization, and, consequently, should display similar irreversible characteristics. Following the discovery, the giant magnetostriction was observed also in single crystals of other HTSC materials [3], thus establishing the effect as being a general phenomenon which, like the magnetization, can provide important information about the pinning properties.

Magnetostriction, as dilatations in general, are most frequently measured by displacive sensors like, e.g., a capacitance dilatometer cell. Such sensors provide an electrical signal which normally represents the variation in the end-to-end dimensions of a sample [4]. Although very high sensitivities (10^{-12} m) can be achieved, the cells are usually designed so that distortions in shape are not accounted for, or they may even influence the measurements in an uncontrolled way. Until now, shape distortions in connection with the pinning-induced magnetostriction were never considered, and all data analysis has been based on the relation [Eq. (1)] valid for plane strain deformations only.

In this Letter, we show that the pinning-induced stress indeed leads to significant shape distortions even in the simple geometry of an infinitely long isotropic cylinder with square cross section. For comparison, we also present the exact solution of the magnetoelastic problem for the circular cylinder where shape is conserved.

From electrodynamics, the force which drives the vortices into the material is given by $\mathbf{j} \times \mathbf{B}$ per unit volume. For HTSCs in the mixed state under practical conditions, the current density $\mathbf{j}$ is usually set equal to $(\nabla \times \mathbf{B})/\mu_0$ as the thermodynamic field can be well approximated by $\mathbf{B}/\mu_0$ [5]. In the critical-state model, one has $|\mathbf{j}| = j_c$, and a nonuniform distribution of pinned flux transmits onto the crystal a volume force density equal to $\mathbf{f} = \mathbf{j}_c \times \mathbf{B}$. In the two geometries under consideration, the symmetry of the force field is quite different (see Fig. 1). In contrast to the simple radial distribution shown in Fig. 1(a), the square cylinder in Fig. 1(b) is divided into four regions each containing distributed forces pointing the same direction. Moreover, in both cases the cylinder generally has additional divisions into shells where the forces alternate in sign—or they can even vanish—all depending on the magnetic prehistory. In all such states, the force exerted on the material per unit volume is given by

$$\mathbf{f} = (\nabla \times \mathbf{B}) \times \mathbf{B}/\mu_0 = -(2\mu_0)^{-1}\nabla B^2. \quad (2)$$

The last form, expressing a purely magnetic free energy of the vortex lattice, is used in the present calculations. In the analysis, the strains are assumed well below the fracture limit allowing linear elasticity theory, and hence the principle of superposition, to be applicable.
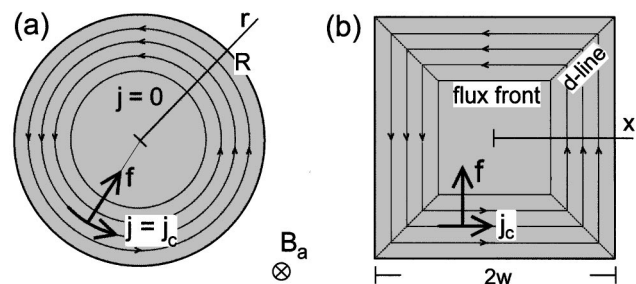

FIG. 1. Flux penetration and current flow pattern in a circular (a) and square (b) cylinder in the critical-state model. The indicated magnetized states contain a flux front, illustrating that the cylinders generally are divided into shells with different volume forces.

In the circular cylinder, the rotational symmetry implies that the deformation is described by a radial displacement field $u_r(r)$. The nonvanishing components of the strain are $e_r = u_r'(r)$ and $e_\theta = u_r/r$, which are related to the stress components σ_θ and σ_r by $Ee_r = \sigma_r - \nu\sigma_\theta$ and $Ee_\theta = \sigma_\theta - \nu\sigma_r$. Here E and ν are the Young's modulus and Poisson's ratio, respectively. The condition of static equilibrium is that $(d\sigma_r/dr) + (\sigma_r - \sigma_\theta)/r + f = 0$, which in terms of the displacement field is expressed as

$$u_r'' + \frac{1}{r} u_r' - \frac{1}{r^2} u_r + \frac{1 - \nu^2}{E} f(r) = 0. \quad (3)$$

Integration twice, and using $u_r(0) = 0$, gives

$$u_r(r) = -\frac{1 - \nu^2}{E} \frac{1}{r} \int_0^r r' F(r') \, dr' + Cr, \quad (4)$$

where $F(r) \equiv \int_0^r f(r') \, dr' = [B^2(0) - B^2(r)]/2\mu_0$. With the constant C determined by the free surface condition $\sigma_r(r = R) = 0$, the result becomes

$$u_r(r) = -\frac{1 - \nu}{2E\mu_0} \left\{ \left[B_a^2 - \frac{1 - \nu}{R^2} \int_0^R r' B^2(r') \, dr' \right] r - \frac{1 + \nu}{r} \int_0^r r' B^2(r') \, dr' \right\}, \quad (5)$$

which is the exact solution from which a complete stress-strain picture can be expressed in terms of the flux density $B(r)$. For example, the radial stress is given by

$$\sigma_r(r) = \frac{1}{2\mu_0} \left\{ B^2(r) - B_a^2 + \frac{1 - \nu}{R^2} \left[\int_0^R r' B^2(r') \, dr' - \frac{R^2}{r^2} \int_0^r r' B^2(r') \, dr' \right] \right\}. \quad (6)$$

Equations (5) and (6) generalize expressions for u_r and σ_r derived recently [6] only for the Bean model, $j_c(B) =$ const. We emphasize that our results are valid for any critical-state model.

For the external dilatation $\Delta R/R = u_r(R)/R$, one obtains from Eq. (5)

$$\frac{\Delta R}{R} = \frac{1 - \nu}{E\mu_0 R^2} \int_0^R r[B^2(r) - B_a^2] \, dr. \quad (7)$$

This formula for the pinning-induced magnetostriction of a circular cylinder, first found by Johansen et al. [7], is very similar to the expression in Eq. (1) for the slab. The extra factor r in the integral is a simple modification, which one finds analogously in the expressions for the critical-state magnetization. The factor $1 - \nu$ reflects the stronger constraint on free expansion for the cylinder as compared to the slab.

From Eq. (7), analytical expressions for the various branches of magnetostriction hysteresis loops are readily derived. Figure 2 shows how $\Delta R/R$ depends on the applied field for two commonly used critical-state models. As B_a runs through a complete cycle, $\Delta R/R$ displays a huge hysteresis loop, where, in the Bean model case, both the main ascending and descending branches are linear provided a sufficiently high maximum field. Among other features of the Bean model results is that the maximum remanent magnetostriction is given by

$$(\Delta R/R)_{\text{rem}} = (1 - \nu)(12E)^{-1}\mu_0 j_c^2 R^2. \quad (8)$$

Since the remanent state has no contribution from reversible components, the above relation provides a means to infer j_c from magnetostriction measurements. In the field range where the main branches are linear, the vertical width of the hysteresis loop equals

$$(\Delta R/R)_\downarrow - (\Delta R/R)_\uparrow = 2(1 - \nu)(3E)^{-1}Rj_c B_a. \quad (9)$$

Note, in particular, that if the hysteresis width is normalized by $(\Delta R/R)_{\text{rem}}$, the value of j_c can be found from the

slope in a plot versus B_a without knowledge of the elastic constants. The normalized width is simply $8B_a/\mu_0 j_c R$, a result analogous to the extensively used Bean model relation between j_c and the width of the magnetization loop. Moreover, once j_c is known, measurements of magnetostriction will also allow determination of the elastic parameter $(1 - \nu)/E$.

The more curved hysteresis loop resulting from the exponential model, $j_c = j_0 \exp(-|B|/B_0)$ [graph (2) in Fig. 2], is usually a better description of observed magnetostrictive behavior in HTSCs [3,8]. An extensive analysis with various $j_c(B)$ functions is the subject of a forthcoming paper, where the rather lengthy expressions for the different branches in Fig. 2 are also presented.

A final remark on the circular case is that the integral in Eq. (7) also can be written as $\int_0^R r^2 f(r) \, dr$; i.e., the
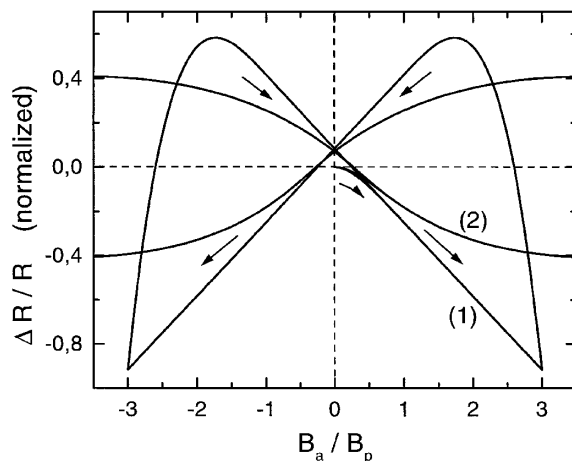

FIG. 2. Magnetostriction, $\Delta R/R \times (1 - \nu)(\mu_0 j_0 R)^2/E\mu_0$, as a function of the applied field for a circular cylinder with $j_c = j_0 \exp(-|B|/B_0)$. Curve (1) $B_0 = \infty$, i.e., the Bean model, and (2) $B_0 = \mu_0 j_0 R/0.3$. The field axis is normalized by the full penetration field $B_p = B_0 \ln(1 + \mu_0 j_0 R/B_0)$.

$\Delta R/R$ is given as the second moment of the volume force distribution just as the j_c loops determine the magnetization. One could be tempted to generalize the relation to other cylindrical geometries, and thus allow for a simple unified treatment as done in magnetization calculations [9]. However, such generalization would be incorrect, as will become evident as we now turn to the square cross-section case.

A different approach is chosen to analyze the magnetoelastic problem of the square cylinder. Within the linear elasticity approximation, one can separate the treatment into an infinite number of deformations produced by infinitesimal square loops of the force field [Fig. 1(b)]. The final result is obtained by superimposing the elastic response of the whole cylinder to each force loop. For this to be a useful approach, one needs a way of adding these deformations in a coherent manner. We first show that this indeed is feasible for the square cylinder.

Consider the effect of a square force loop of width dx with sides a distance x from the origin (Fig. 3). The material enclosed by the loop will experience only a normal stress, and the deformation becomes a plane strain. The elastic response of the enclosed area is given by $Ee_1 = \sigma_1 - \nu\sigma_2$ and $Ee_2 = \sigma_2 - \nu\sigma_1$, where e_1, e_2 and σ_1, σ_2 are the plane strain and normal stress components, respectively. It immediately follows that the relative change in the square area equals $e_1 + e_2 = -(1 - \nu)E^{-1}2p$, where $p = -(\sigma_1 + \sigma_2)/2$ is the two-dimensional pressure. The enclosed area deforms under this pressure into another square so that a constant gap δg is created along the loop. Using $p = -f(x)\,dx$, the size of this virtual gap becomes

$$\delta g = -(1 - \nu)E^{-1}xf(x)\,dx. \qquad (10)$$

The sign of δg is so that a positive value represents a void space, whereas a negative δg corresponds to an expansion of the inner square.

The contribution from this elementary deformation to the strain of the whole body is obtained by recombining (gluing together) the parts on each side of the virtual gap. The resulting strained state is equivalent to having a pair of edge dislocations in each corner of the loop. As each pair can be replaced by one dislocation directed along the diagonal, we conclude that the original gap space can be replaced by two slits of width $\delta G = \delta g\sqrt{2}$ forming a central cross. By this transformation, the integral effect of the entire force field can be determined analytically as follows.

Let y denote the distance from the center to a point on a diagonal. At this point, the total gap G is an accumulation of the gaps δG created from y and out to the corner $y = w\sqrt{2}$. The total result is therefore given by

$$\frac{G(y)}{w\sqrt{2}} = \frac{1 - \nu}{E\mu_0 w}\int_{y/\sqrt{2}}^{w} B(x)B'(x)x\,dx. \qquad (11)$$

The full deformation is now obtained by "gluing" the virtually disrupted material together. Since $G'(y) \propto$

$Bj_c y$, it follows that $G(y)$ is not a constant, thus proving that the pinning-induced magnetostriction does not conserve shape in the square case.

Equation (11) allows the gap to be calculated. In the Bean model along the increasing field branch, one finds for $\tilde{G} \equiv GE\mu_0 6(1 - \nu)^{-1}B_p^{-2}$ the expression

$$\frac{\tilde{G}(y)}{w\sqrt{2}} = 3\left[1 - \left(\frac{y}{w\sqrt{2}}\right)^2\right]$$
$$\times \left(\frac{B_a}{B_p} - 1\right) + 2 - 2\left(\frac{y}{w\sqrt{2}}\right)^3, \qquad (12)$$

in the penetrated region. In the central Meissner area, the gap is constant. The behavior is shown in Fig. 4(a), and representative examples of the resulting concave deformations are illustrated qualitatively in Fig. 3(b). For the fully penetrated state, one sees from Eq. (12) that $G(y)$ grows linearly with B_a, while at the same time $G = 0$ at the corners. This produces a deformation
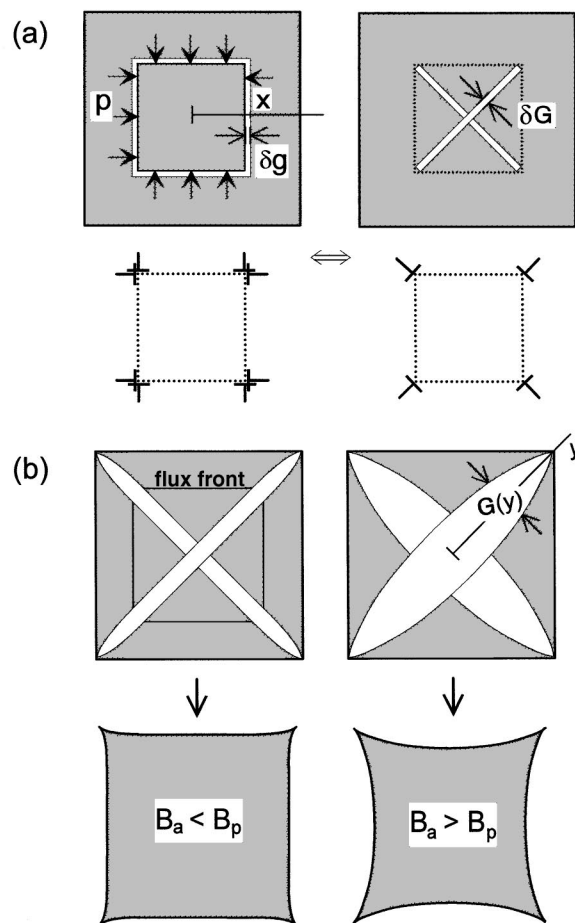

FIG. 3. (a) Partial effect of the volume force in a square cylinder. By the shown transformation, the elastic problem can be treated analytically using superposition (see text). (b) Schematic picture of the deformation (strongly amplified) of a square cylinder in the case of (left) incomplete and (right) complete flux penetration.
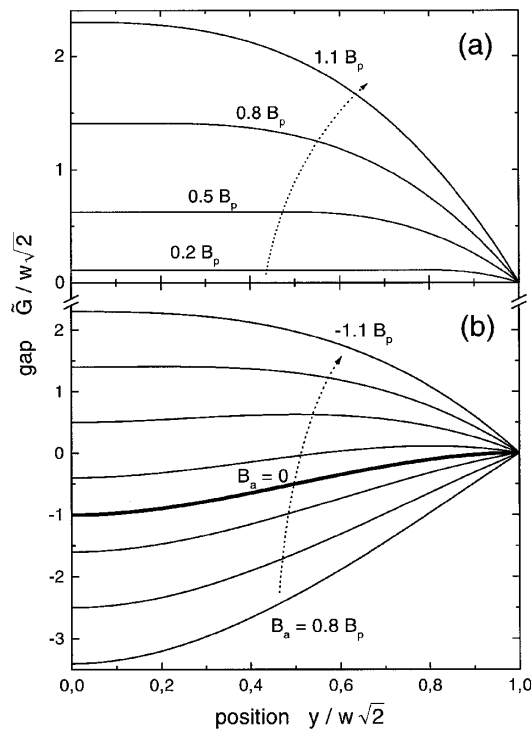
FIG. 4. Gap shape at various stages of flux penetration. (a) Increasing field (B_a indicated) and (b) decreasing field for $B_a/B_p = 0.8$, 0.5, 0.2, 0 (thick line), -0.2, -0.5, -0.8, and -1.1.

where the concave character grows steadily with the applied field.

The behavior of $\tilde{G}(y)$ for descending applied field is shown in Fig. 4(b). The deformation along this branch is evidently more diverse even when we omit the stage following immediately after field reversal. The shown graphs represent only stages where j_c is reversed throughout the sample. The profiles with negative $\tilde{G}$ give rise to convex deformations. The convexity persists all the way down to the remanent state, where the distortion near the corners is vanished. Then, as the field is reversed, there is an interval where the behavior is governed by a $G(y)$ with an oscillatory shape, thus giving a mixed type of deformation. As the reverse field increases in magnitude, the shape again becomes concave. For $B_a \leq -B_p$, the sample shape follows the same development as during the field increase.

One can easily envisage that the pinning-induced strains also influence the overall superconducting properties of a bulk sample. As observed, e.g., by magneto-optical imaging, such samples usually contain one or more extended defects which in effect divide the sample into several parts as far as flux penetration is concerned. After applying an external magnetic field, the connectivity between parts which deform with consid-

erable shape distortion is likely to degrade significantly. Thus, we expect that the magnetostriction could be an important factor limiting the intergranular critical current density.

In conclusion, we have investigated and compared the pinning-induced magnetostriction in two important geometries. In contrast to the shape-conserving circular case, which could be solved exactly, the existence of current discontinuity (d) lines in the square case complicates the behavior by producing shape distortion. We have predicted the appearance of convex, concave, and even more complicated types of deformations, where the distortion is of the same order of magnitude as the overall striction. Since in most cases HTSC crystals have a rectangular shape, which always leads to d lines in the critical state, the distortion could easily cause a misinterpretation of dilatometric measurements. The problem should be minimized by (i) having a high aspect ratio rectangular shape so that the central part of the sample is described approximately by a plane strain deformation, and (ii) designing the displacive sensor with only a *local* contact to the long side of the rectangle in order to avoid the distorted corner regions. Full analysis of the proper corrections will clearly require numerical work.

[1] H. Ikuta, N. Hirota, Y. Nakayama, K. Kishio, and K. Kitazawa, Phys. Rev. Lett. **70**, 2166 (1993).

[2] G. Brändli and R. Griessen, Phys. Rev. Lett. **22**, 534 (1969); G. Brändli, Phys. Kondens. Mater. **11**, 93 (1970).

[3] N. Hirota *et al.,* J. Supercond. **7**, 283 (1994); A. Schmidt *et al.,* Physica (Amsterdam) **194B–196B**, 1787 (1994); A. Nabialek *et al.,* Supercond. Sci. Technol. **10**, 786 (1997).

[4] R. Jones and J. Richards, J. Phys. E **6**, 589 (1973); G. Brändli and R. Griessen, Cryogenics **13**, 299 (1973); T. H. Johansen, J. Feder, and T. Jössang, Rev. Sci. Instrum. **57**, 1168 (1986).

[5] E. Zeldov, J. R. Clem, M. McElfresh, and M. Darwin, Phys. Rev. B **49**, 9802 (1994).

[6] Y. Ren, R. Weinstein, J. Liu, R. P. Sawh, and C. Foster, Physica (Amsterdam) **251C**, 15 (1995).

[7] T. H. Johansen, J. Lothe, and H. Bratsberg, in *Fourth Euro-Ceramics—High T_c Superconductors, Part II,* edited by A. Barone, D. Fiorani, and A. Tampieri (Gruppo Editoriale Faenza Editrice, Faenza, Italy, 1995).

[8] H. Ikuta, K. Kishio, and K. Kitazawa, J. Appl. Phys. **76**, 4776 (1994).

[9] D.-X. Chen and R. B. Goldfarb, J. Appl. Phys. **66**, 2489 (1989); T. H. Johansen and H. Bratsberg, J. Appl. Phys. **77**, 3945 (1994).